Welding in the World (2018) 62:497–509
https://doi.org/10.1007/s40194-018-0576-8

RESEARCH PAPER

Application of hybrid friction stir channeling technique to improve the cooling efficiency of electronic components

Heikki Karvinen[1] · Daniel Nordal[1] · Timo Galkin[2] · Pedro Vilaça[1]

Received: 12 September 2017 / Accepted: 3 March 2018 / Published online: 22 March 2018

Abstract
Hybrid friction stir channeling (HFSC) is a new friction stir-based method for producing internal, closed channels created simultaneously during welding of multiple metal plates. Differently from conventional friction stir channeling, that is only able to produce channels in a monolithic component, HFSC can be applied to complex structural systems involving multiple components made of similar or dissimilar materials. In this study, the channels manufactured by HFSC were open in a structural system made of AA5083, with one base plate of 5 mm thick, and one overlapping plate of 8 mm thick, used as a rib, containing the channel along conformal cooling path. The thermal performance of the HFSC channel is compared with a conventional channel, with similar shape and path, produced by milling. The channels being tested are part of an electronic device containing multiple heat sources. The HFSC channel presents 30 to 40% lower steady-state temperature and 33% higher cooling rate during the transient period than those of the milled version. Compared with the milled channel, the heat extraction capacity, per unit of mechanical pumping power, is higher for the HFSC channel. Surface roughness, microhardness, and microstructural analysis of HFSC channels are investigated to characterize the HFSC channel.

Keywords Friction stir processing · Solid-phase welding · Heat exchanger · Thermal properties · Electronic devices · Aluminum alloys

1 Introduction

Hybrid friction stir channeling (HFSC) is a new friction stir-based process characterized by producing a channel and a weld simultaneously by a rotating non-consumable tool. During the HFSC, the tool applies simultaneously solid-state joining and material extracting mechanisms into the materials within the stirred processed zone, wherein the channel and the weld between at least two material components are produced in one single and simultaneous action. This process was submitted by Vilaça et al. for national patent in 2016 [1] and international PCT in 2017 [2]. As prior art of HFSC, Mishra proposed in 2005 friction stir channeling (FSC) as a manufacturing method for small heat exchangers [3]. Mishra's concept was based on reversing the material flow pattern from friction stir processing, which enabled production of internally closed channel within a monolithic plate. In the concept, all material extracted in the process is laid on a small clearance between the tool shoulder and workpiece. Therefore, the final surface is higher than the original surface. Later, in 2009, Balasubramanian et al. [4] presented the characterization of these channels. Rashidi et al. [5] reported similar FSC concept with modifications in the tool design and positioning. Instead of threaded tool probe as in Mishra's concept, Rashidi et al. channeled aluminum with smooth cylindrical probe with a tilt angle and non-threaded conical probe without a tilt angle and with a clearance between the shoulder and the workpiece [6]. In all these solutions, the size of the channels is limited because the material is kept in the processing domain, and the gap with the tool has to be small in order to keep the channel closed. In 2013, Vilaça et al. [7] patented a new concept of the original FSC of monolithic components, which was based on a distinct material flow where controlled amount of processed material is extracted from the processed

Recommended for publication by Commission III - Resistance Welding, Solid State Welding, and Allied Joining Process

✉ Heikki Karvinen
heikki.karvinen@aalto.fi

[1] Department of Mechanical Engineering, School of Engineering, Aalto University, 02150 Espoo, Finland

[2] Nokia, 02610 Espoo, Finland

zone as self-detaching flash. In this concept, the tool shoulder is kept in contact with the surface of the workpiece, and thus, the processed surface is planar and at the same dimension as the original surface. By adjusting process parameters and tool features, it is possible to produce channels with wide range of dimensions. These channels are addressed by Vilaça et al. [8] and extensively characterized by Vidal et al. [9–11]. A significant benefit of using HFSC is that the channel can be produced in component systems involving thin workpieces, made of the same or different materials, instead of the thick monolithic preforms required in the FSC concepts.

The constantly developing electronic applications are a high potential field of application for the HFSC because it requires improved cooling solutions to maintain operational temperatures of the components. Increasing power density limits usability of air cooling systems due to the low efficiency of convective heat transfer in air. Heat transfer coefficient of water in forced convection can reach 1000 W/m^2 K whereas the heat transfer coefficient of air is around 5 W/m^2 K in natural convection and 25 W/m^2 K in forced convection [12]. Conventional passive and active air cooling solutions are not enough to dissipate heat from high local hot zones. Selecting materials with high thermal conductivity has a limited cooling effect because the whole heat transfer path affects the total thermal resistance [13]. Increased temperatures reduce the reliability of the electronic components and require large cooling structures, which prevents utilizing the miniaturization possibilities of novel electronics. Liquid cooling is already applied for electronics and electrical applications such as data centers [14], personal computers [15], frequency transformers [16], and electric motors [17]. The high efficiency of liquid cooling enables significant space savings since the components can be positioned close to each other and large air condition devices are not needed. Heat energy can also be recovered and reused to heat buildings or even generate electricity depending on the level of heat energy available.

Liquid cooling is already implemented and researched for cooling of enclosures of electronic devices [18] or direct cooling of the electronic chips by micro-channels [19]. Micro-channels are channels with hydraulic diameters ranging 10–200 μm fabricated for example by micromachining, sawing, or etching [20]. There are many methods to produce flow paths of liquid-cooled applications within a single or multiple operations. These include but are not limited to drilling, milling, electric discharge machining (EDM), 3D printing, extruding, tubing, casting, and welding of pre-manufactured profiles. Some methods are not suitable for complex channel paths such as drilling, EDM, and extruding. On the other hand, milled channels require closing operations by welding, screwing, brazing, or gluing. 3D printing enables production of very complex structures, but currently, the manufacturing speed and expensive materials hinder implementing 3D printing. Use of tubes in a heatsink is a common solution, but that increases the thermal resistance of the system due to the additional interface between the tube and heatsink. The quality of the interfaces along the heat transfer path affects the cooling efficiency. Microgaps and macrogaps in the interface between two solids are commonly filled by substances (air, water, grease) whose thermal conductivities are much smaller than those of the contacting solids [12].

In this research, the effect of the channel geometry is studied by measuring cooling efficiency of liquid-cooled heatsinks having similar channel shape and dimension made by HFSC and milling. The purpose is to analyze the effect of surface finishing and the shape of the HFSC channel to the milled channel having relatively smooth surface quality. Analysis is based on the ability and efficiency of the heatsinks to cool a prototype of electronic device with multiple heat sources. In addition, the quality of HFSC channel is assessed with microhardness testing and optical microscopy. Microhardness testing and optical microscopy are used to evaluate changes in mechanical and microstructural properties due to thermomechanical processing.

2 Features and application of hybrid friction stir channeling

Hybrid friction stir channeling (HFSC) is a recently developed manufacturing method for internally closed channels created simultaneously during welding of multiple metal components. HFSC is based on processing of metal with a non-consumable tool in a visco-plastic state, which allows flow of solid metal. The visco-plastic state of metal is also utilized in other friction stir-based techniques to join materials by friction stir welding (FSW) [21], to deposit material layers on a plate by friction surfacing (FS) [22], to modify material properties by friction stir processing (FSP) [21], and to create internally closed channels into a monolithic plate by friction stir channeling (FSC). HFSC combines the benefits of FSW and FSC into a single stable process. With a suitable design of the probe and shoulder, the material flow is used to mix and forge an interface of two or more metal components forming a weld and creating an outward material flow forming a channel. The shoulder design assures the closing of the roof of the channel and the generation of detachable flash, for any volume of material extracted. The channel and weld produced simultaneously with this method can have a path of any shape and the cross-sectional area of the channel is constant or continuously modifiable along the path. The possibility to join components during channeling allows producing channeled structures from thin preforms. The tetragonal-like cross-section of the HFSC channels has internal irregular surface finishing that increases the surface area, promotes turbulent flow even at low flow rates, and thus potentially improves heat transfer between solid material and fluid. In addition, HFSC does not

require consumables or additional supporting chemicals in production, such as many other alternative channeling techniques. No fumes or radiation are generated making HFSC a friendly process for the environment and the operator.

The geometrical arrangement of the multiple components in the joint can be designed in an overlap joint, butt joint, or a combination of overlapped and butt joints as shown in Fig. 1b. Figure 1a shows the concept of HFSC applied on three overlapped components along a non-linear path. HFSC concept reduces the material requirements of channeled applications since only the material volume required by the channel is added during processing, e.g., as a rib element. This also minimizes the post-processing since other geometrical features of the component can be produced before the HFSC. In HFSC, the probe creates a combined action, to weld the workpieces and flow part of the stirred material against the shoulder. The geometrical features of tool shoulder are kept in contact with the workpiece generating combined actions to seal the roof/ceiling of the channel and to extract a variable amount of material as a flash. The processed surface is therefore at the same level than the original surface. The process is controllable and repeatable and is able to produce channels with a wide range of dimensions, by controlling the process parameters. For comparison purposes, the geometries of conventional FSC and HFSC channel cross-sections are shown in Fig. 2. Figure 2a shows a FSC channel made into monolithic thick plate made of aluminum AA6082-T651. Figure 2b shows a HFSC channel produced within the interface of two thick AA5083-H111 plates. Both channels have similar overall shape features, namely, the advancing side (AS) and bottom of the channel which are straighter and the surface is smoother than those in the retreating side (RS) and ceiling of the channel.

The present study is concentrated on aluminum because the behavior of the material flow of aluminum is well known from other friction stir-based techniques, and aluminum can be processed with low-cost tooling. Clamping is important in HFSC concept, mainly when material ribs are joined to a pre-manufactured workpiece that is not allowed to be deformed during the HFSC processing.

3 Experimental methods

3.1 Materials and general characterization conditions

Experimental analysis of HFSC channels included microhardness testing, microstructural analysis of processed zone, and testing of cooling efficiency. Channels for microhardness testing and optical microscopy were made of 5- and 8-mm-thick overlapping plates of aluminum alloy AA5083-H111. This material is good for thermal management applications due to its good corrosion resistance and strength [23]. Although the nominal magnesium content of 4.5% reduces its strength at high temperatures [24], the typical level of operation temperatures during thermal management is typically below 100 °C, and thus, this characteristic is not a limitation for the envisaged application. The composition of AA5083-H111 is shown in Table 1.

The plates were fixed with steel clamps on the worktable of an ESAB Legio FSW 5U machine. In the overlapping arrangement, the 5-mm plate was on the bottom and the 8-mm plate on top. Three M5 screws were used to bolt the plates together near the starting point of the channel to prevent the lifting effect during plunging of the HFSC probe. The lifting of the plates may occur if the plates are not clamped firmly and processed material is able to flow between the plates. The HFSC tool used had a probe with an envelope diameter of 10 mm. The tool was plunged 9.5 mm deep in the thickness of the component system, until the 22 mm in diameter shoulder contacted the top surface of the plates. HFSC was produced with position control. The tool rotation speed was 800 rpm during plunging and 300 rpm during traveling at 90 mm/min. The dwell time of 2 s was applied after plunging and before tool accelerated in 3 s into the specified travel speed.

Samples for microhardness testing and optical microscopy were cut from 210-mm long channel using a Beka-Mak BMSY 32CGL saw and a Struers Discotom-50 circular saw. The Vickers microhardness testing was applied with a Struers Duramin-A300 hardness tester and 500 gf. The indentation spacing was 1 mm and hardness was measured across the base material and the processed zone. Hardness of unprocessed

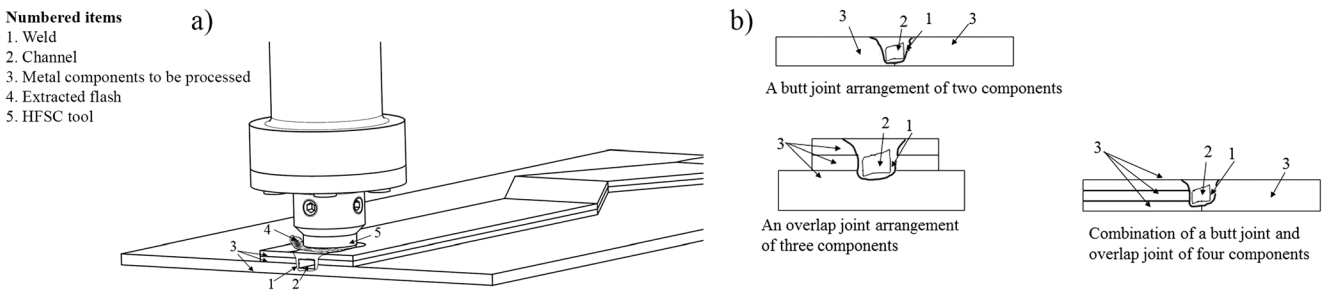

Fig. 1 Concept of HFSC with **a** HFSC applied to three overlapped components along a non-linear path and **b** schematic representation of alternative joints for HFSC

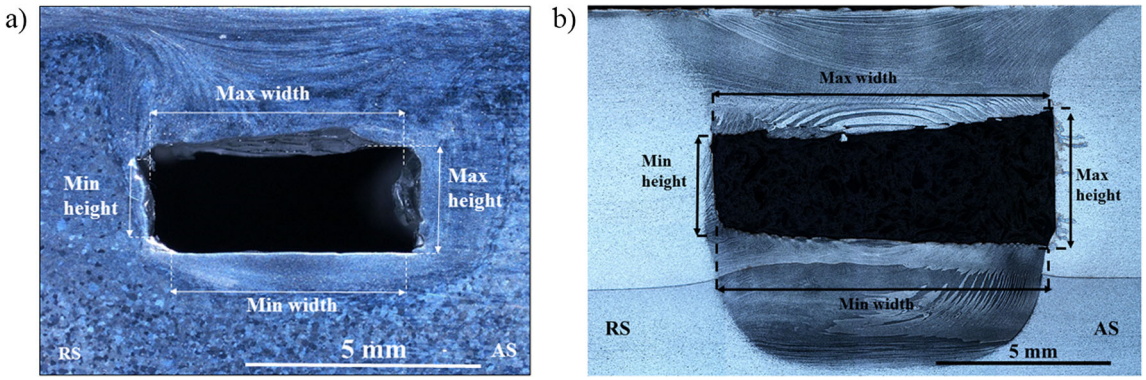

Fig. 2 Macrographs of channel cross-sections of **a** conventional FSC channel produced in thick plate AA6082-T651 and **b** HFSC channel produced within the interface of two AA5083-H111 plates

base material samples with thicknesses of 5 and 8 mm was also measured. The indentation matrix for the hardness mapping of HFSC is shown in Fig. 3. Samples for microhardness testing and microstructural analysis were cold mounted using Struers VersoCit-2 Kit acrylic resin. Sample for hardness testing was ground on a Struers LaboPol-21 machine using SiC papers to a 4000 grit finish and polished with 3-μm diamond compound on a Struers LaboPol-5 machine.

Optical microscopy sample was further polished with a 1-μm diamond compound. The sample was etched using a 10% hydrofluoric (HF) acid. After microscopy analysis, the channel was repolished to a 1-μm finish and etched using modified Poulton's solution. Microstructural investigation was carried out optically with a Nikon Epiphot 200 microscope equipped with a Nikon DS-2Mv camera. The microscopic analysis focused on the weld nugget, channel ceiling, and the four corners of the channel within the thermomechanically affected zone (TMAZ). The microstructural zones are shown in Fig. 2b.

Surfaces of the channels were scanned optically with ATOS Triplescan 3D scanner to analyze the surface features more closely. The scanning was based on stereo camera technique that includes a source of blue light and two cameras. Part of the HFSC channel was cut in two pieces by wire cutting with a wire diameter of 0.3 mm so that the top and bottom surfaces of the channel were accessible for the scanner. A section of an open-milled channel was scanned. The length of the pieces of the channel samples were 15 mm. The samples were painted with matt gray spray paint before scanning to avoid errors from reflections. The 3D scanned samples were processed and analyzed with GOM Inspect software.

Cooling efficiency of HFSC channels was measured with a prototype of liquid-cooled heatsink representing an enclosure of a small electronic device. Principal dimensions of the prototype were 170 mm × 140 mm × 60 mm. Two heatsink prototypes were made, with one containing a HFSC channel and the other containing a milled channel with a screwed lid to seal the roof of the channel. The cooling channel in both prototypes had the same 465-mm long flow path with similar overall shape. In addition to the heatsink, the prototype assembly included a printed wiring board (PWB), thermal interface materials, six power resistors as heat sources, and a plastic top cover to prevent airflow over the resistors.

3.2 Procedure for cooling efficiency testing

Cooling performance was measured with steady-state and transient conditions. Steady-state condition was measured with fixed total heat power of 65 W at different volume flow rates: 0.3, 0.5, 0.8, 1.0, 1.5, 2.0, and 2.5 l/min. The Reynolds number was used to enable the adimensional comparison between the two similar, but not equal, channels produced by HFSC and milling. The Reynolds number is calculated with Eq. (1).

$$\mathrm{Re} = \frac{\rho v L}{\mu} \tag{1}$$

in which the ρ is the density (kg/m^3) of the fluid, v is the flow velocity (m/s) of the fluid, L is the wetted perimeter (m) of the channel, and μ is the viscosity (kg/(m.s)) of fluid. In practical terms, the wetted perimeter is the perimeter of the channel in contact with the fluid.

The flow is laminar at the small Reynolds number and the heat is transferred by molecular conduction between fluid particles. At the large Reynold number, the flow

Table 1 Material composition of AA5083-H111 [24]

Al	Mn	Fe	Cu	Mg	Si	Zn	Cr	Ti
Balance	0.4–1.0	≤0.4	≤0.1	4.0–4.9	≤0.4	≤0.25	0.05–0.25	≤0.15

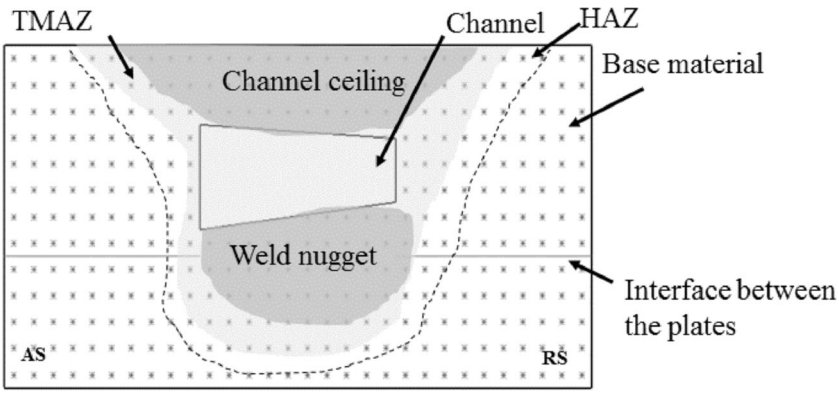

Fig. 3 The indentation matrix used in the hardness testing and microstructural zones of the processed region. Indentation spacing 1 mm. HAZ heat-affected zone, TMAZ thermomechanically affected zone

becomes turbulent and the particle are mixed, which increases heat transfer [25]. For a given volume flow rate $\dot{V}$ (m^3/s) and rectangular channel cross-section, Eq. (1) can be rearranged into Eq. (2).

$$\mathrm{Re} = \frac{\rho \nu L}{\mu} = \frac{\frac{4 \cdot A}{L} \cdot \frac{\dot{V}}{A} \cdot \rho}{\mu} = \frac{4\,\dot{V}\rho}{L\mu} \tag{2}$$

in which A is the cross-sectional area of the channel. Parameters L for the HFSC and milled channel are 0.0244 m and 0.0236 mm, respectively. The parameter L for HFSC channel is calculated with image processing software. The water-ethylene glycol mixture is approximated to have density of 1.023 kg/m^3 and dynamic viscosity of 0.001 kg/(m.s).

Steady-state conditions were reached when the temperature in measurement locations varied less than 0.5 °C during 1000 s. Temperature was logged every 10 s. At a heat power of 65 W, three measurements were made at each flow rates.

Three transient cooling tests were made for both prototypes at 30.7-W heating power. The prototypes were heated to steady-state condition without flow rate. After stable conditions, liquid cooling was turned on with a fixed flow velocity of 0.56 m/s for both prototypes and temperature was monitored and logged at a 5-s interval until conditions were stabilized. Cooling rates of the channels were calculated with Eq. (3).

$$C = \frac{\Delta T}{\Delta t} \tag{3}$$

in which the T is temperature of the heatsink and t is time. Results are calculated as average from three measurements.

The closed flow circuit in the test consisted of a 7-l liquid container, pump, hoses, digital flowmeter, analog pressure gauge, and a heat exchanger to transfer the heat from the system into air. The system kept the inlet temperature of the liquid approximately at room temperature. Illustration with components of the system is shown in Fig. 4.

3.3 Manufacturing of HFSC prototype

The HFSC heatsink prototype was manufactured from 5- and 8-mm-thick plates. To simulate the rib concept, the 8-mm-thick channeled plate was milled with a machining center to the final shape before assembling hose couplings, heat sources, sensors, and top cover. Hose couplings for the HFSC prototype were manufactured from M10 stainless steels screws with 5-mm hole through the screw and making 90° before entering the channel. The hose couplings were attached with a nut and washer plates. Manufacturing sequence of the HFSC prototype and the hose coupling are shown in Fig. 5.

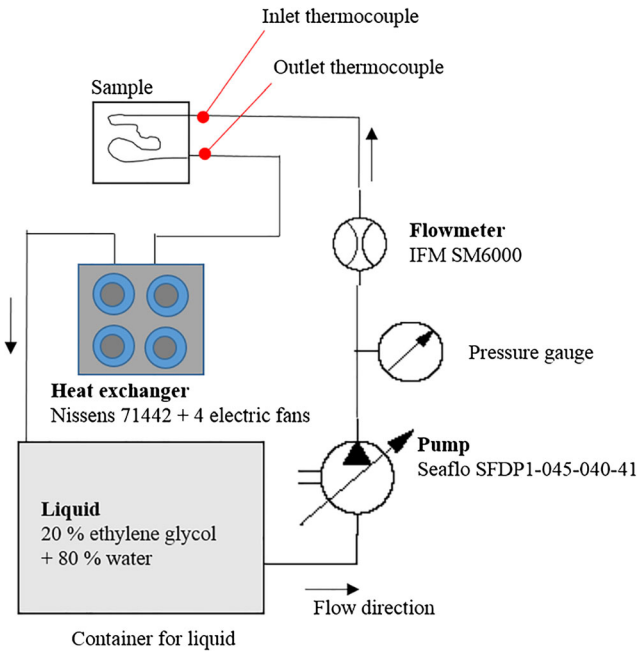

Fig. 4 Illustration of the test setup for liquid cooling

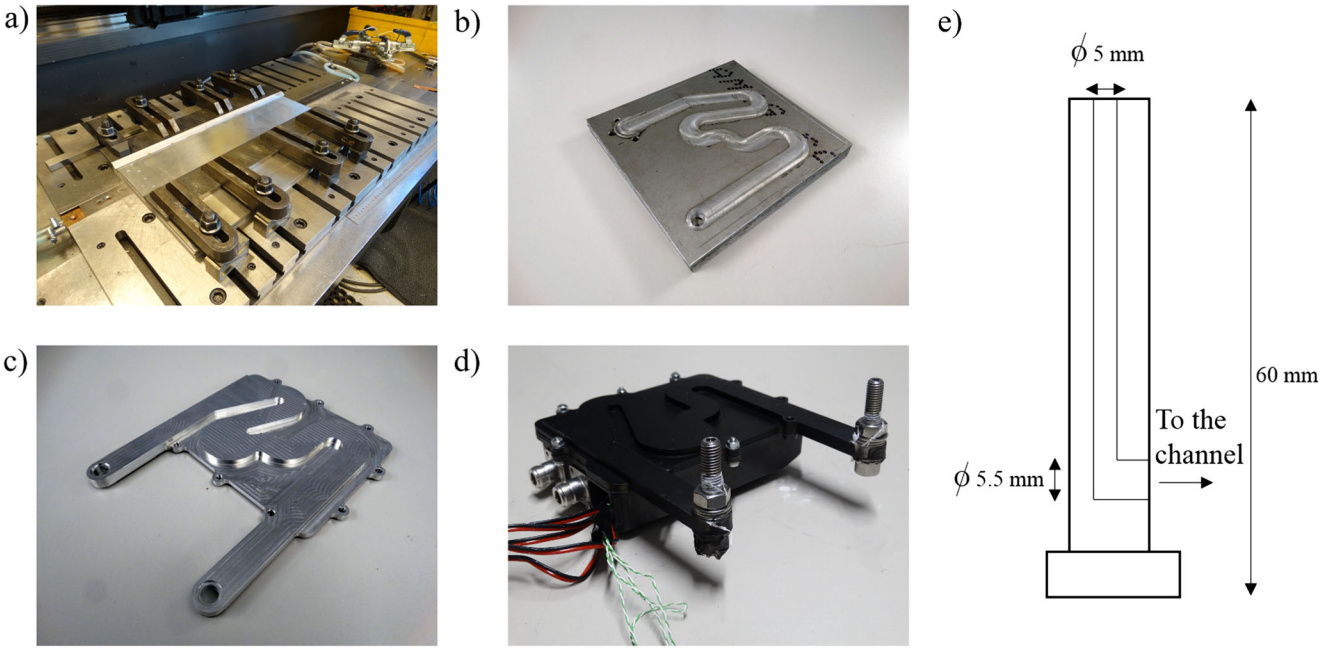

Fig. 5 Manufacturing process of the HFSC prototype showing **a** clamping of 5- and 8-mm plates for HFSC process, **b** plates with weld and channel after HFSC, **c** HFSC prototype after milling the shape of the device, **d** the assembled prototype, and **e** illustration of the hose coupling used with HFSC channel

The cross-sectional area of the HFSC channel was measured to be 26.1 mm^2.

3.4 Manufacturing of the prototype with milled channel

The prototype with milled 2.5 × 9.3-mm channel was machined from a single aluminum plate. The milled rectangular groove having the same flow path as the HFSC channel was covered with a 2-mm-thick aluminum plate. The lid was sealed with 47 M3 screws and Hylomar® M jointing compound. Conventional straight hose spindles attached with R 1/8 pipe threads were used with the milled channel. The channel profile and the prototype are shown in Fig. 6.

Both production methods resulted in heatsinks with admissible distortion, easy to assemble to the chassis containing the electronic components.

3.5 Heat source

Six ARCOL HS25 power resistors were used as heat sources representing actual electronic components such as processors and flash memories (Fig. 7a). Similar heat source arrangement was prepared for both prototypes. One resistor was attached with two M3 screws to the liquid-cooled heatsink and five resistors were screwed with M3 screws to a printed wiring board (PWB). Thermally conducting silicon paste was used to seal the interface when attaching the resistors. Silicon-filled

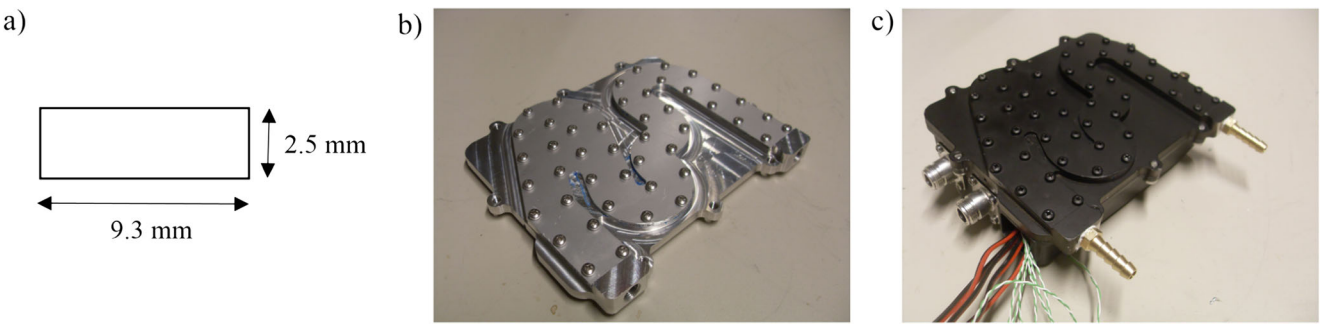

Fig. 6 The prototype with the milled **a** rectangular channel having dimension of 2.5 mm × 9.3 mm, **b** the prototype after sealing the channel with a screwed lid, and **c** the assembled prototype

Al_2O_3 gap pads were used to secure the contact between the PWB and the heatsink (shown as blue rectangles in Fig. 7b). Tests were run with a heat power level of 65 W in steady-state testing and 30.7 W in transient-state testing.

3.6 Thermocouple locations

Four K-type thermocouples (Labfacility Z2) were used to measure the temperature of heatsink, liquid inlet, liquid outlet, and ambient. The thermocouple in the heatsink was attached by gluing into a 2 × 2-mm groove under the 22-Ω resistor. Horizontal and vertical locations of the thermocouple in the heatsink is shown in Fig. 7. The heat flux of the resistor was 5.0 W/cm^2 at the steady-state testing and 2.2 W/cm^2 at the transient testing. During steady-state testing, temperature was logged at 10-s intervals. In transient testing, temperature was logged at a 5-s interval.

4 Analysis of results

4.1 Microhardness

During HFSC, processing material is subjected to large shear deformation affecting the microstructure and mechanical properties. Changes in mechanical properties were evaluated with hardness testing. The average hardness of 5- and 8-mm-thick unprocessed base material samples were 98 and 98.5 HV05, respectively. A microhardness map of the HFSC sample is shown in Fig. 8. The horizontal line presents the interface between the 5- and 8-mm plates. The dark blue zones in the middle and at the horizontal line come from the channel and the interface gap, respectively. There is increased hardness in the weld nugget and in individual zones in the channel ceiling. The average hardness of the HFSC sample was 106 HV05 with a maximum value of 125 HV05 and a minimum value of 98 HV05. Hardness reduced in the TMAZ and heat-affected zone on both sides of the channel. There is a slight increase in the hardness on the RS comparing to the AS.

4.2 Microstructural characterization

Microscopic image of the HFSC channel is shown in Fig. 9. Figure 9a depicts the whole HFSC processed zone and Fig. 9b shows detailed view of the weld zone of the HFSC. The comparison between AS and RS interface zones reveals a significant difference in the transition of grain size and orientation. The AS has a very narrow and well-defined boundary or transition zone observed as a crisp boundary between the recrystallized region and the TMAZ. On the RS, this region is much larger and less well defined, because the transition from the base material's large grain structure to the processed zone's small recrystallized region takes place within a wider layer. This increased size in the grain transition zone is caused by the higher energy transported via the RS during the material flow.

The wavy line shown in weld stirred zone is the processed original oxide layer interface between the plates. The oxide layer of the aluminum plates are strong and stable and they need to be broken and stirred efficiently to produce strong welds. Lack of deformation and mixing of the oxide layers can result in a weaker joint. It can be seen in Fig. 9b that the original oxide layers are more mixed in AS. Other critical zones of the processed region are marked as rectangles in Fig. 9a, namely the corners of the channel, ceiling stirred zone of the channel, and weld stirred zone. The microstructure of these zones is presented in Fig. 10a–h.

The grain distortion and flow characteristics of RS are observable in a more detailed way in Fig. 10a, d. Corresponding zones on AS are shown in Fig. 10c, e. Figure 10a, c presents a clear transition between the TMAZ, with distorted grain structure, and the stirred zone, that is completely recrystallized with

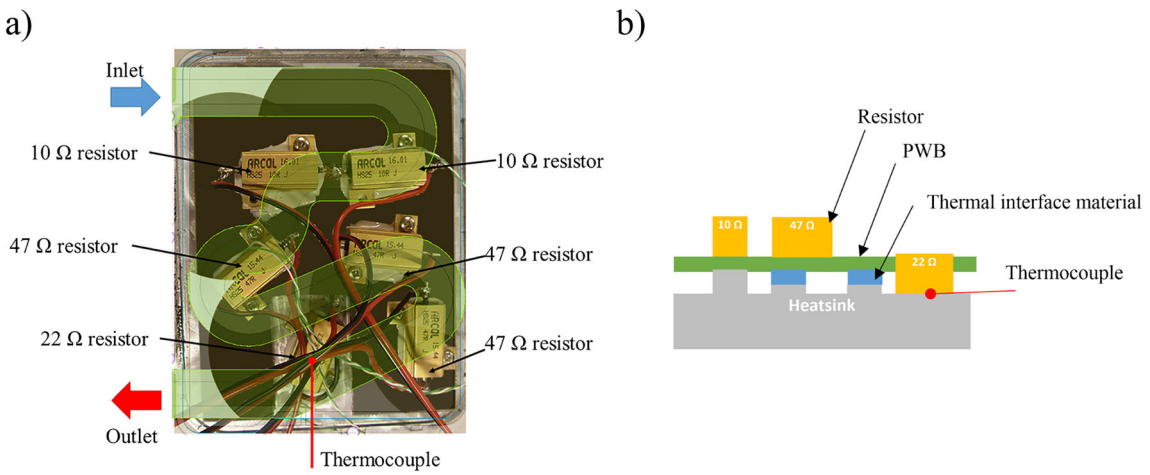

Fig. 7 Heat sources, thermocouple location, and the channel path of the prototypes from **a** top view and **b** schematic side view

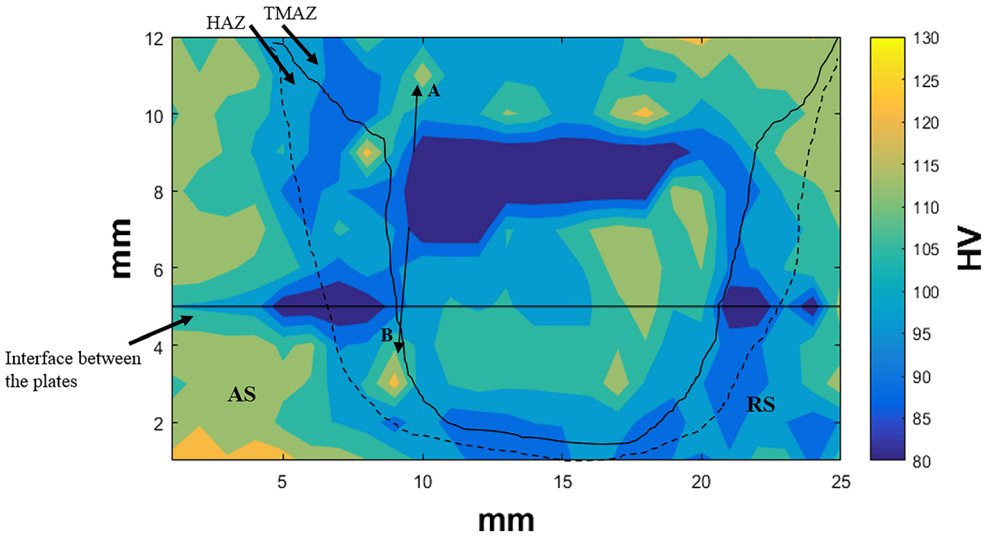

Fig. 8 Microhardness mapping (HV05) of the channel and weld zone produced during HFSC. Arrow A and arrow B identify hardness gradient in important zones at the AS near the interface between TMAZ and HAZ

a refined grain structure due to severe plastic deformation and heating. It can also be observed that the TMAZ adjacent to the channel is distorted in an upward direction on the RS near the channel ceiling (Fig. 10a). The distortion curves back down as the channel ceiling interface moves outwards away from the channel. This causes the localization of a material flow inflection point in the RS and channel ceiling corner resulted from a two-directional material flow. The material flow is produced from the probe extracting material from the processed zone while the shoulder forges material back into the top of the channel. The AS of the channel is presented in Fig. 10e where it is possible to see that the extracted material from the channel left only a very narrow recrystallized region adjacent to the inner channel surface. In contrast, Fig. 10d exhibits a RS of the channel with wider layer of stirred material. The localized character of the shear deformation enacted on the AS of the channel results in a smother finishing of that surface. Another localized material flow inflection point is located in the RS at the interface with the weld stirred zone (Fig. 10f) resulting from a multidirectional material flow. The material flow is caused by the channeling section of the probe extracting material upwards to the shoulder and the welding tip forging the weld stirred zone. Due to an increased amount of material flow from the AS to the RS in the weld stirred zone and RS of the channel, the lower material flow inflection point is localized at the interface between the TMAZ and weld stirred zone.

Examination of the middle of channel ceiling (Fig. 10b) and weld stirred zone (Fig. 10g) reveals significant recrystallization and grain refinement. The weld stirred zone contains a higher level of grain refinement observed by the finer grain structure although the overall difference is small. This suggests a higher heat input and slower cooling rate in the weld stirred zone over the channel ceiling allowing for finer grain formation. With the weld located close to the mid-thickness of the component system, it will experience a faster cooling rate than the channel ceiling further supporting the findings of the finer grain structure in the weld stirred zone.

HFSC is a new process, demanding investigation of the multiple physical aspects, affecting its performance. One of the important issues is related with the mechanical resistance properties and susceptibility to cracking under fatigue loading. In this regard, the combined analysis of the microstructural

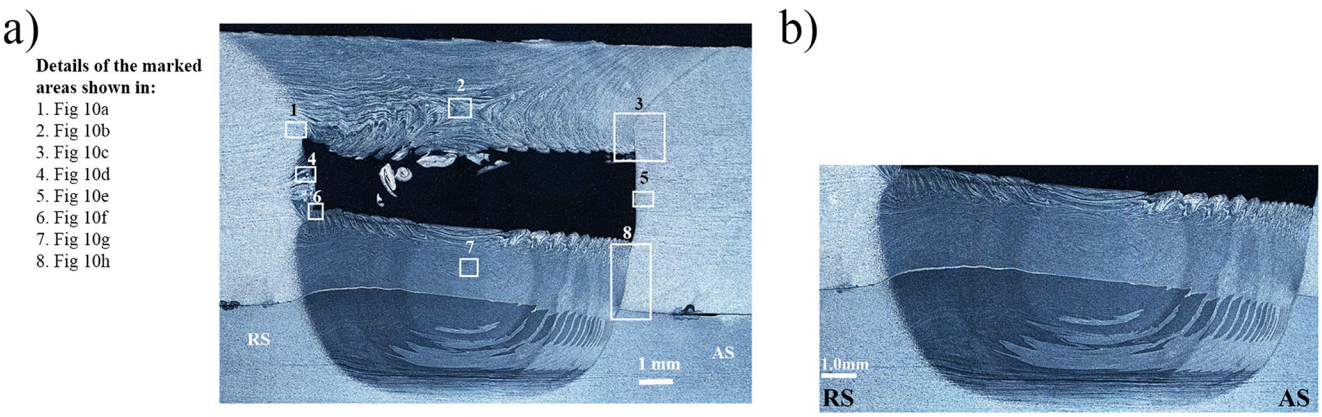

Fig. 9 Microstructure of the channel produced with HFSC present as **a** macrograph (etched with 10% HF) of all channel area and **b** detail with weld stirred zone

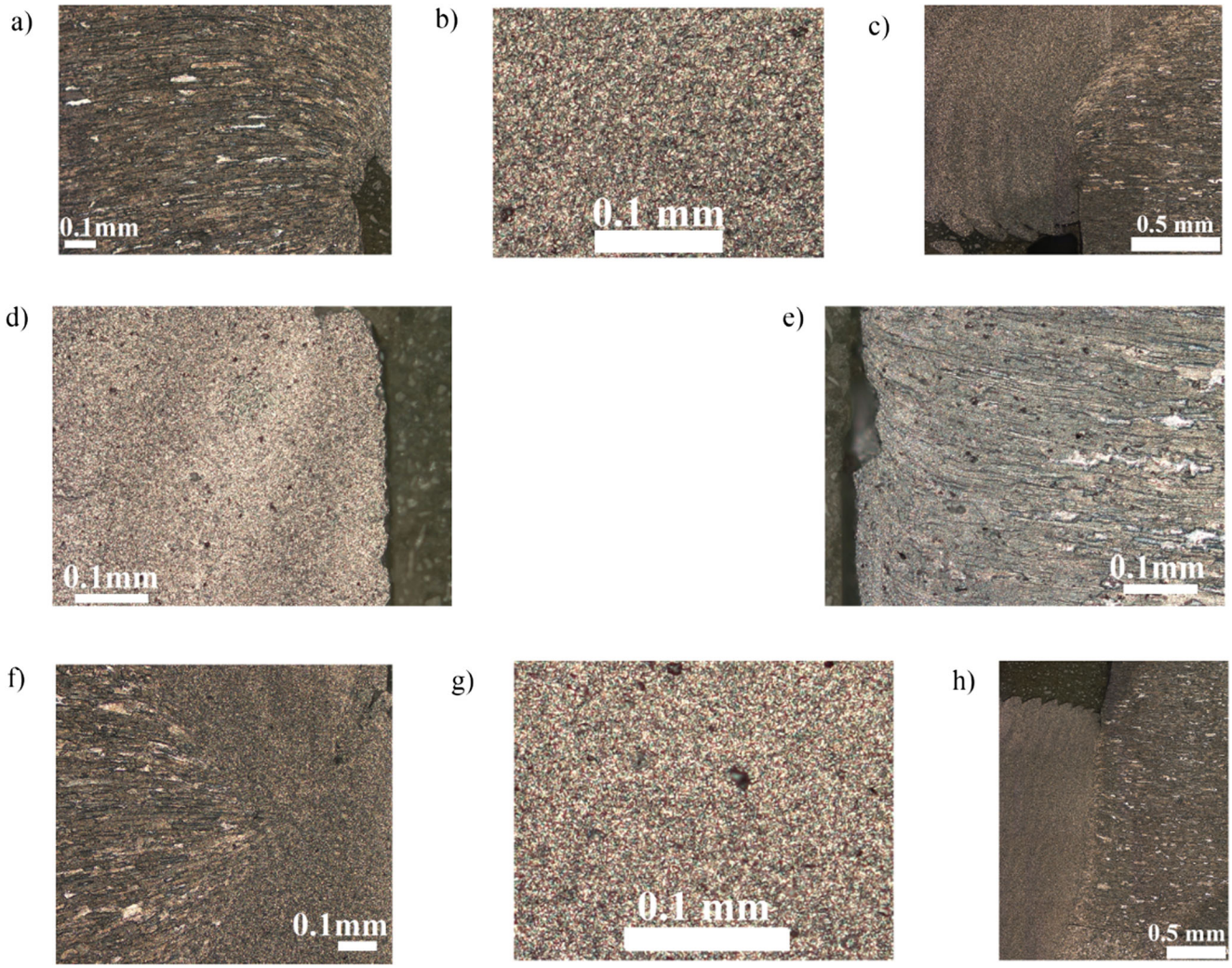

Fig. 10 Micrographs (etched with modified Poulton's acid) of the critical zones identified in Fig. 9a, namely **a** RS—channel ceiling interface, **b** channel ceiling stirred zone, **c** AS—channel ceiling interface, **d** RS, **e** AS, **f** RS—weld stirred zone interface, **g** weld stirred zone, and **h** AS—weld stirred zone interface

characterization (Fig. 10) and the hardness field (Fig. 8) enables a preliminary identification of potentially critical zones. The corners at the ceiling of the channel, presented in Fig. 10a (at the RS) and Fig. 10c (at the AS), are geometrically similar to the ones resulting from application of conventional FSC. These zones were investigated by Vidal et al. [9–11], reporting that the fracture under fatigue loading of all specimens took place in the interface at the AS, corresponding to the notch of Fig. 10c. The same studies conclude that this interface is a region of stress intensity between very fine and coarse grains that is amplified by the channel corner geometry, and a mix fracture mode of intergranular decohesion and transgranular cracking was globally observed, although it was found that at 200 °C, intergranular decohesion tends to replace transgranular cracking. Additionally to the conventional FSC, the HFSC presents one more potentially critical interface, located in the AS of the weld stirred zone, presented in Fig. 10h. The hardness field presented in Fig. 8 brings up some important additional information, about the mechanical behavior of these interfaces between TMAZ/HAZ, located at the top (Fig. 10c) and bottom (Fig. 10h) corners of the channel. There is a local hardness increase, from about 85 to 120 HV at both the top and bottom of the channel corners identified as arrows "A" and "B," respectively. This fact may contribute for a better mechanical performance. These combined effects, the identified microstructural zones and other features of HFSC, are under research to characterize the mechanical properties of HFSC.

4.3 Channel surface analysis

Results of the surface scanning are shown in Fig. 11. Figure 11a shows the surfaces of the milled channel. The surface is relatively smooth with an overall roughness height of 1–10 μm and with some peaks having a height of 20–50 μm. Similar surface quality is observed from all the surfaces. Figure 11b, c shows

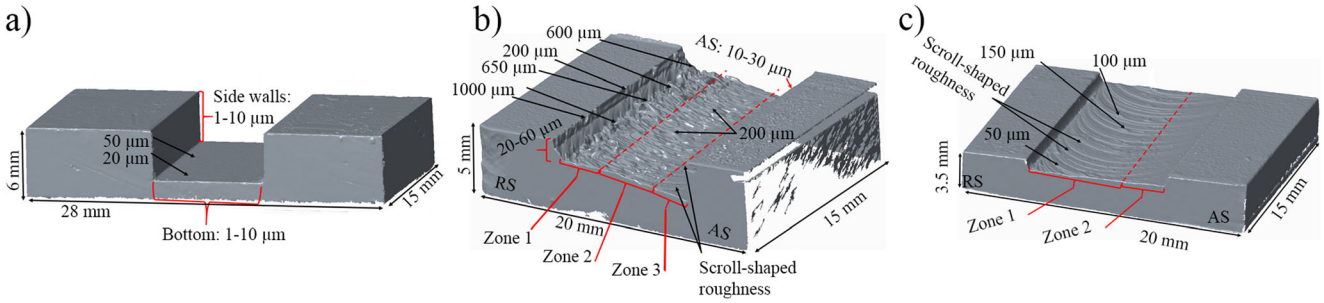

Fig. 11 3D models constructed from the optical scanning to analyze the surface roughness of **a** a milled channel, **b** top surface of the HFSC channel, and **c** bottom surface of the HFSC channel

the top and bottom surfaces of the HFSC channel, respectively. The overall roughness and the height of the peaks are higher than those of the milled channel. There are identified repetitions of scroll-shaped roughness that originates from the rotating tool. This pattern is visible on the top, bottom, and side surfaces of the channel. The top and bottom surfaces of the HFSC channel are rougher and there are more irregular peaks near the RS than near the AS. The overall height of surface roughness on the RS is 20–60 µm and there are some peaks with the height of 200–240 µm. The roughness of the AS is in the range of 10–30 µm with some peaks having the height around 60–80 µm. There are identified different roughness zones from the top and bottom parts of the HFSC channel. On the top surface of the channel, there are three defined zones from RS to AS:

1. Zone 1: An overall roughness of 150–300 µm; roughness peaks up to 1000 µm;
2. Zone 2: An overall roughness of 70–150 µm; roughness peaks up to 200 µm;
3. Zone 3: An overall roughness of 10–30 µm; no significant roughness peaks.

The bottom surface is generally smoother than the top surface. In the bottom surface, the material flow created by the probe is not restricted as much as on the top surface. On the top surface, the pressure applied by the shoulder creates a two-directional material flow that closes the ceiling of the channel and forms the rough surface. Two different zones are observed:

1. Zone 1: An overall roughness of 20–60 µm; roughness peaks up to 150 µm;
2. Zone 2: An overall roughness of 10–30 µm; no significant roughness peaks.

4.4 Cooling efficiency

Figure 12 shows the results of the cooling tests, namely, the temperature of the thermocouple in contact with the heatsink (Fig. 7b) as a function of the Reynolds number. Temperatures are shown as a difference from ambient temperature. Temperature at the liquid inlet was monitored and is included in Fig. 12a. The HFSC channel keeps the temperature of heatsink lower than the milled channel, at all the tested flow rates. Based on Fig. 12a, the temperature of the heatsink follows the changes in the inlet temperature. This fact can be seen in the results for milled channel where the heatsink temperature seems to stabilize or increase around the Reynolds number of 2500. At steady-state conditions, the temperature difference between the heatsink and

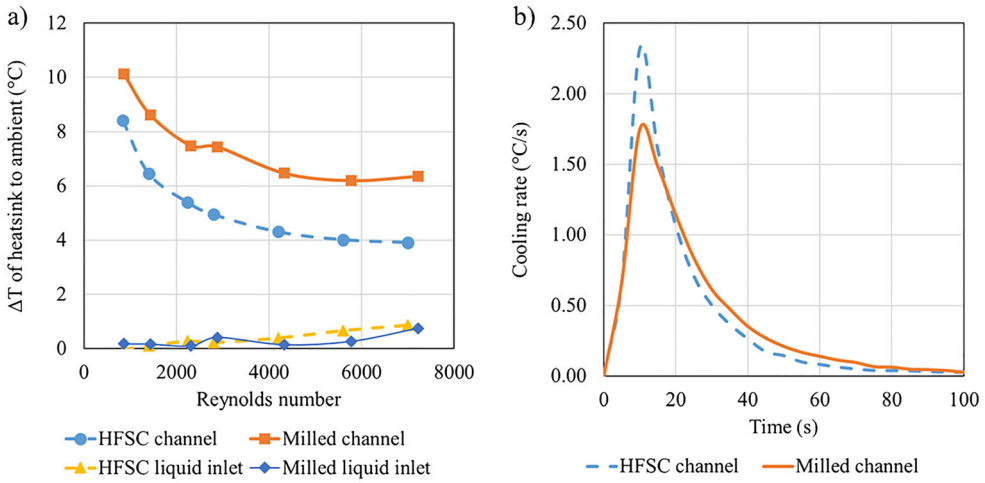

Fig. 12 Results of the cooling tests in terms of the **a** temperature of the heatsink as function of the Reynolds number at 65 W of total heating power and **b** transient cooling performance of the liquid-cooled channels at a flow velocity of 0.56 m/s and a total heating power of 30.7 W

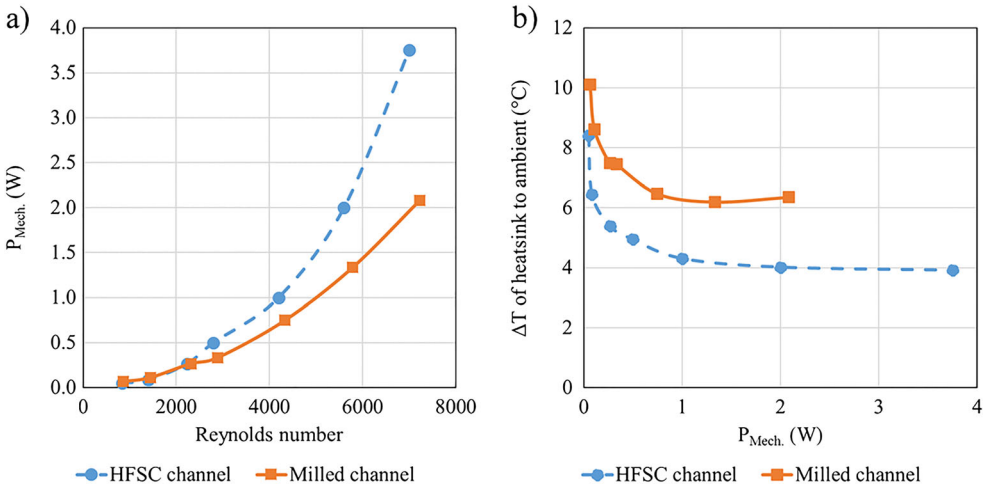

Fig. 13 Mechanical power requirement for the pump to flow the fluid vs. **a** the Reynolds number and **b** temperature of the heatsink

ambient was 30 to 40% lower in HFSC than in milled prototype. The difference between HFSC and milled channel increased with increasing flow rate. Approximately, after the Reynolds number of 1700, the temperature of the heatsink with the HFSC channel was lower than that in the heatsink with the milled channel, at all range of flow rates tested.

Results of the transient-state testing are shown in Fig. 12b. The maximum cooling rates of the HFSC and milled prototypes are 2.32 and 1.75 °C/s, respectively, which represent 33% higher cooling rate for the HFSC prototype. The high cooling rate is important for cooling systems that need to be responsive for changing conditions. High responsive cooling system can effectively cool sudden increases in heat fluxes and increase service life of electronics.

The shape and geometry of the channel and the used hose couplings of the HFSC increase flow resistance compared to that of milled channel, which can be seen in the mechanical power requirement presented in Fig. 13. The mechanical power $P_{Mech.}$ is calculated with Eq. (4).

$$P_{Mech.} = p \cdot \dot{V} \tag{4}$$

in which the p is the pressure (Pa) of the flow and $\dot{V}$ is the volume flow rate (m^3/s).

More mechanical power is required for HFSC at all flow rates and the difference increases with increasing flow rate. Increasing requirement of mechanical power indicates that the differences of the surface roughness of the milled and HFSC channel shown in Fig. 11 affect the flow behavior. The overall roughness and the random peaks are higher and more irregular in the HFSC channel than in the milled channel, which increases instability of the flow and promotes turbulence at lower flow rates. At the Reynolds number of 2000, the difference is not significant, but at the Reynolds number of 6000, the pressure in HFSC channel is 50% higher than in milled channel. By comparing the requirement for mechanical power and the Reynolds number, the HFSC prototype requires more energy to operate the flow (Fig. 13a).

However, when analyzing the temperature of the heatsink versus the mechanical power (Fig. 13b), the HFSC channel cools the electronic components more efficiently at all levels of mechanical power, e.g., for the power of 0.5 W, the temperature difference between the HFSC channel and ambient is 30% lower than that between the milled channel and ambient. Emphasis should be given to the fact that at low values of mechanical power (e.g., 0.15 W), the level of cooling reached with the HFSC prototype is already better than the cooling reached with the milled channel at any level of mechanical power. This means that although the HFSC channel presents higher pressure loss during fluid flow, even with low mechanical pump power, the cooling efficiency already overcomes the milled channel in all range of pump power.

In general, the results show that by increasing the flow rate, the power requirement increases significantly, but it does not improve cooling.

5 Conclusions

The following conclusions can be drawn from the work presented before:

- The HFSC showed to be a feasible technique to produce closed internal channels of large dimensions, with complex path, while joining two overlapped plates. All in one action only.
- Microhardness testing showed increase of hardness of the weld stirred zone compared to that of base material. The TMAZ and HAZ present the lower hardness values, but matching the base material original conditions. Some important gradients exist along the interface between TMAZ

and HAZ, at the AS, protecting the geometrical notches at the top and bottom corners of the channel.

- Based on the microstructure analysis, the uniform layer of recrystallized stirred material in the channel ceiling and high gradient of vertical packed layers of stirred material against the sheared wall at the AS is evidence of good consolidation of the joining mechanisms that close the channel. The homogenous and wide zone of the weld stirred zone, although containing some aligned oxide layer, is evidence of a sound weld between the overlapping components of the heatsink produced with the HFSC.
- The overall roughness and the height of the peaks are higher than those of the milled channel. In average, comparing the roughness of the HFSC channel with the roughness of the milled channel, in the HFSC channel, the roughness at top and bottom are 20 and 10 times higher, respectively. The roughness of the HFSC channel is not uniform, presenting more irregular peaks near the RS than near the AS.
- The HFSC channel presents in overall better cooling performance when compared with similar channels produced by milling. Considering that the channels have the same shape and path, it must be the geometric features of the HFSC channel, that makes the difference. Even at very low mechanical pumping power, the HFSC channel enable to reach better cooling efficiency than the milled channel, at any mechanical power level.
- During the transient cooling period, the HFSC-based solution presented a faster cooling rate. The fast cooling response reducing the peak temperatures represents a feature of high importance for extending the life of electronic components that undergo complex and demanding heat loading cycles during service;
- At steady-state conditions, temperature difference between the heatsink and ambient was 30 to 40% lower in HFSC than in milled heatsink prototype.

Acknowledgements The authors acknowledge the support from The Finnish Funding Agency for Innovation (TEKES) via the program: New knowledge and business from research ideas—TUTL.

References

1. Vilaça P, Karvinen H FI patent applications FI 20160165 and FI 20160247, 23 June 2016
2. Vilaça P, Karvinen H, Nordal D Patent Application: PCT/FI2017/050467, 21 June 2017, 2017
3. Mishra RS (2005) Integral channels in metal components and fabrication thereof, US6923362 B2
4. Balasubramanian N, Mishra RS, Krishnamurthy K (2009) Friction stir channeling: characterization of the channels. J Mater Process Technol 209(8):3696–3704
5. Rashidi A, Mostafapour A, Salahi S, Rezazadeh V (2013) Modified friction stir channeling: a novel technique for fabrication of friction stir channel. Appl Mech Mater 302:365–370
6. Rashidi A (2015) Influence of tool pin geometry and moving paths of tool on channel formation mechanism in modified friction stir channeling technique. Int J Adv Manuf Technol 80(5–8):1087–1096
7. Vidal C, Vilaça P Processo de Abertura de Canais Internos Contínuos em Componentes Maciços Sem Alteração da Cota da Superfície Processada e Respetiva Ferramenta Modular Ajustável, PT 105628, 21 June, 2013
8. Vilaça P, Gandra J, Vidal C (2012) Linear friction based processing technologies for aluminum alloys: surfacing, stir welding and stir channeling, in Aluminum Alloys—New Trends in Fabrication and Applications, Z. Ahmad, Ed. InTech, pp. 159–197
9. Vidal C, Vilaça P, Infante V (2012) Mechanical characterization of friction stir channels under internal pressure and in-plane bending. Key Eng Mater 488-489:105–108
10. Vidal C (2014) Fatigue assessment of friction stir channels. Int J Fatigue 62:77–84
11. Vidal C (2015) Characterisation of fatigue fracture surfaces of friction stir channelling specimens tested at different temperatures. Eng Failure Anal 56:204–215
12. Bejan A, Kraus AD (2003) Heat transfer handbook. Wiley, New York 1479 p
13. Drofenik U, Stupar A, Kolar JW (2011) Analysis of theoretical limits of forced-air cooling using advanced composite materials with high thermal conductivities. IEEE Trans Compon Pack Manuf Technol 1(4):528–535
14. Iyengar M, David M, Parida P, Kamath V, Kochuparambil B, Graybill D, Schultz M, Gaynes M, Simons R, Schmidt R, Chainer T (2012) Server liquid cooling with chiller-less data center design to enable significant energy savings. In: 2012 28th annual IEEE semiconductor thermal measurement and management symposium (SEMI-THERM), pp 212–223
15. Abbas T, Abd KM, Khodairy K (2010) CPU thermal management of personal and notebook computer (transient study). In: 2010 3rd international conference on thermal issues in emerging technologies theory and applications, pp 85–93
16. Zaidi A, Hussin N, Maizana D (2015) Palm oil as the cooling liquid in single phase transformer for better efficiency. Appl Mech Mater 793:192–196
17. Davin T, Pellé J, Harmand S, Yu R (2015) Experimental study of oil cooling systems for electric motors. Appl Therm Eng 75:1–13
18. Nörtershäuser D, Le Masson S, Volkov T, Huttunen J, Douchet F (2014) Liquid cooling for mobile base station, in 36th International Telecommunications Energy Conference (Proceedings), Vancouver, Canada pp. 1–8
19. Kroeker CJ (2004) Three-dimensional thermal analysis of heat sinks with circular cooling micro-channels. Int J Heat Mass Transf 47(22):4733–4744
20. Kandlikar SG, Grande WJ (2003) Evolution of microchannel flow passages—thermohydraulic performance and fabrication technology. Heat Transfer Eng 24(1):3–17
21. R. S. Mishra and Z. Y. Ma, Friction stir welding and processing, Mater Sci Eng, vol. 50, (1), pp. 1–78, 2005
22. Klopstock H, Neelands AR (1945) An improved method of joining or welding metals, GB 572789 A
23. Dwight J (1999) Aluminium design and construction. London, UK: E & FN Spon, an imprint of Routledge, 314 p

24. ThyssenKrupp Materials (UK) Ltd. (2017, May 23). Aluminium Alloy 5083-O H111—Material Data Sheet. Available: http://www.thyssenkruppmaterials.co.uk/Downloads/Download_Files/Aluminium_Datasheets/5083-O H111.pdf

25. Yeh L (2016) Thermal management of microelectronic equipment. (2nd ed.). The American Society of Mechanical Engineering, New York 492 p